Title

MRI-guided high-intensity focused ultrasound ablation of bone: evaluation of acute findings with MR and CT imaging in a swine model.

Journal

Journal of magnetic resonance imaging : JMRI, 40(5)

ISSN

1053-1807

Authors

Bucknor, Matthew D
Rieke, Viola
Do, Loi
et al.

Publication Date

2014-11-01

DOI

10.1002/jmri.24451

Peer reviewed

Published in final edited form as:
J Magn Reson Imaging. 2014 November ; 40(5): 1174–1180. doi:10.1002/jmri.24451.

MR GUIDED HIGH-INTENSITY FOCUSED ULTRASOUND ABLATION OF BONE: EVALUATION OF ACUTE FINDINGS WITH MR AND CT IMAGING IN A SWINE MODEL

Matthew D. Bucknor, MD[1], **Viola Rieke, PhD**[1], **Loi Do, BS**[1], **Sharmila Majumdar, PhD**[1], **Thomas M. Link, MD, PhD**[1], and **Maythem Saeed, PhD**[1]

[1]Department of Radiology and Biomedical Imaging, University of California San Francisco, 185 Berry Street, Suite 350, San Francisco, CA 94107-5705, United States

Abstract

Purpose—To evaluate hyperacute (<1 hour) changes on MR and CT imaging following MR guided high-intensity focused ultrasound (MRgHIFU) in a swine bone model as a function of sonication number and energy.

Materials and Methods—Experimental procedures received approval from the local institutional animal care and use committee. MRgHIFU was used to create distal and proximal ablations in the right femur of eight pigs. Each target was dosed with 4 or 6 sonications within similar volumes. The energy dosed to the distal target was higher (419±19 J) than the proximal target (324±17 J). The targeted femur and contralateral control were imaged before and after ablation using MR at 3T. Qualitative changes in signal on T1-weighted, T2-weighted,, and T1-weighted postcontrast images were assessed. Ablation dimensions were calculated from postcontrast MR imaging. 64-slice CT images were also obtained before and after ablation and qualitative changes were assessed.

Results—MRgHIFU bone ablation size measured on average 8.5 × 21.1 × 16.2 mm (transverse × craniocaudal × anteroposterior). Interestingly, within similar prescribed volumes, increasing the number of sonications from 4 to 6 increased the depth of the intramedullary hypoenhanced zone from 2.9mm to 6.5mm (p<0.001). There was no difference in the appearance of low versus high energy ablations. CT imaging did not show structural abnormalities.

Conclusion—The number of MRgHIFU focal sonications can be used to increase the depth of treatment within the targeted bone. Unlike CT, T2-weighted and contrast enhanced MR demonstrated the hyperacute structural changes in the femur and surrounding soft tissue.

Keywords

MR guided focused ultrasound; high-intensity focused ultrasound; MRI; bone ablation

Corresponding author: Matthew D. Bucknor, MD, Department of Radiology and Biomedical Imaging, University of California, San Francisco, 185 Berry Street, Suite 350, San Francisco, CA 94107-5705, Tel: (415) 353-2450, Fax: (415) 353-0616, matthew.bucknor@ucsf.edu.

INTRODUCTION

Magnetic resonance-guided high intensity focused ultrasound (MRgHIFU) is a powerful technique for thermally ablating focal lesions. MRgHIFU offers multiple advantages compared to other forms of focal ablation including the high precision of energy delivery, the lack of adjacent tissue toxicity, and the completely non-invasive approach (1). The technique is most frequently used to treat uterine fibroids or for palliation of painful bone metastases refractory to radiation therapy (2–6). However, the number of potential applications has rapidly increased over the last decade, with multiple studies examining its use for liver, breast, renal, prostate, and brain tumors, in addition to stroke, peripheral neurolysis, and essential tremor (7–17). HIFU has also been successfully used for treatment of osteoid osteomas (18) and more controversially, for primary bone malignancies (19–23).

The use of MRgHIFU as a therapy for pathologies in and around bone requires negotiating several unique challenges. Sound energy travels through most soft tissues with modest attenuation until it reaches areas of dense mineralization or high collagen content, including fascia, ligaments, tendons, capsule, periosteum, and bone (24). When sound waves reach a bone-soft tissue interface, there is rapid attenuation secondary to reflection, scattering, and mode conversion, in addition to absorption (25). As a result, it is estimated that bone attenuates approximately 60–80% of acoustic energy (26). Additionally, differences in the percentage of cortical versus cancellous bone and woven versus lamellar organization of collagen fibers make bone architecture and its interaction with sound waves, difficult to reliably predict.

While the main focus of MRgHIFU treatment of painful bone metastases has been the ablation of periosteal innervation along the margin of the bone, several studies have suggested the possibility of a meaningful treatment effect at increased depths from the superficial bone-soft tissue interface. Notably, some patients undergoing HIFU for bone metastases have demonstrated focal sclerosis several centimeters deep to the cortical surface on follow-up CT scans (5). Furthermore, HIFU of large primary bone tumors has shown the ability to devascularize large lesions across the full width of bone, with no appreciable contrast enhancement on follow-up studies several years removed from HIFU (21). Finally, early work for intracranial applications of HIFU has found robust means of compensation for calvarial distortion, with precise focusing of ultrasound waves several centimeters deep to the cortical margin of the skull (27,28).

A prior experimental HIFU study at the bone-soft tissue interface suggested that placing the focal spot of the sonication at the superficial (relative to the transducer) or deep bone-soft tissue interface had no significant effect on an ablation along the superficial interface (29). The purpose of this study was to evaluate the hyperacute (<1 hour) appearance of bone on 3.0-T MR and 64-slice multidetector CT imaging following MRgHIFU and to quantify differences in the size of the ablation zone as a function of focal spot number and energy.

MATERIALS AND METHODS

Animal Preparation

All experimental procedures received approval from the Institutional Animal Care and Use Committee (IACUC). This investigation conformed to National Institutes of Health guidelines for the care and use of laboratory animals. Eight healthy female farm pigs (mean weight, 31.0 ± 1.7 kg) (Pork Power Farms, Turlock, CA, USA) were premedicated with 0.5 mg/kg acepromazine [PromAce; Fort Dodge Animal Health, Fort Dodge, Iowa] and 30 minutes later 25 mg/kg ketamine [Ketaset; Fort Dodge Animal Health]). They were then anesthetized with a mixture of isoflurane 2%–5% and oxygen. Saline (10 mL/kg/hr) was intravenously infused throughout the experiment for hydration Vital signs (heart rate, ECG, respiratory rate, O2-saturation) were monitored throughout the procedure.

System Set-up And Planning

An MRgHIFU system (ExAblate2000, Insightec, Haifa, Israel) with a phased array transducer of 208 elements embedded in an MR scanner table was used to create the ablations. The table was connected to an MRI scanner (Discovery MR750w 3T, GE, Milwaukee, WI, USA). In each animal, the skin above the targeted treatment areas in the right femur was shaved, cleaned, and closely examined for any skin defects or scars, which might impede the propagation of acoustic energy from the transducer. Each pig was then placed onto the scanner table in the right lateral decubitus position, inside a shallow bath filled with degassed water, so that the right femur was centered directly above the transducer embedded within the table. A three-plane localizer was then performed to verify adequate position, followed by treatment planning sequences. The skin surface and cortical surface of the bone were manually segmented by the operator with eight years of focused ultrasound experience (VR). Two ovoid ablations measuring 2 cm in craniocaudal dimension were then prescribed on the MR planning images (nonenhanced T2-weighted sequences with fat saturation) along the lateral margin of the right femur at the proximal diaphysis and the distal metadiaphysis. A low-energy test sonication was performed in the adjacent soft tissues to confirm accuracy of the system set-up and the path of the sound waves.

In four animals, each prescribed ablation was manually assigned four sonication focal spots: two adjacent spots overlapping approximately 3 mm in the craniocaudal dimension and a similar set of two spots on the adjacent coronal slice through the right femur (7 mm medial to the original slice) (Figure 1). In the remaining four animals, two additional sonications were assigned within each of the two ovoid ablations (for a total of six sonications per ablation) one additional sonication centered at the midpoint between the two initial sonications, on each of the two treatment slices (Figure 1). In all animals, and for all sonications, the focal spots were similar in size and geometry, measuring up to approximately 1 cm each, with a bean-shaped morphology.

MRgHIFU Treatments

Each focal spot sonication lasted 20 seconds in duration and was performed at a frequency of 1.05 MHz, with a subsequent cooling duration of 25 seconds. In all animals, the average energy assigned to the focal spots to compose the proximal ablation was less than that used

to create the distal ablation in order to demonstrate any associations between energy dose and ablation size. The energy for the proximal focal spots ranged from 300 to 360 J and from 360 to 440 J for the distal ablations. The acoustic power was used to vary the total energy dose with a goal of creating a 7–10° C discrepancy between the proximal (desired temperature increase to 60° C) and distal (desired temperature increase to 67–70° C) ablations. Increases in temperature were monitored using real-time MR thermometry of phase-difference fast spoiled gradient-echo sequences (proton resonant frequency shift method) in the soft tissues immediately adjacent to the targeted bone (30). Operator variations in acoustic power were guided by the real-time MR thermometry readings during test and initial treatment sonications.

MR Imaging

Treatment started by acquiring 2D fast gradient echo localizer (FOV/slice thickness/TR/TE/flip angle=44×744cm/7mm/3500ms/1.5ms/9000b0). The following sequences were acquired at baseline: 3D T2-weighted fast spin echo (FSE) (FOV/slice thickness/TR/TE/flip angle=44×44cm/7mm/3500ms/100ms/90), T1-weighted fast spin echo (FOV/slice thickness/TR/TE/flip angle= 44×44cm/7mm/450ms/min full/not applicable), and 3D spoiled gradient echo images were acquired for treatment planning (FOV/slice thickness/TR/TE/flip angle= 44×44cm/3.8mm/4.3ms/2ms/15). After baseline images the MRgHIFU treatment was performed. MR thermometry was performed during each sonication with multiphase multislice echo planar imaging (FOV/slice thickness/TR/TE/flip angle/echo train length= 28 × 28 cm/4mm/210ms/18.3ms/35/12). The baseline MR sequences were then repeated before and after contrast media administration (0.15mmol/kg Gd-DTPA). In addition, saturation-recovery first-pass perfusion gradient echo images (FOV/slice thickness/TR/TE/flip angle= 48×48cm/7mm/3500ms/83ms/30) were acquired. T1-weighted fast spin echo and spoiled gradient echo sequences were acquired serially over the course of 15min. Quantitative data were obtained from the optimum time of 10 minutes post contrast administration.

CT Imaging

Imaging was performed with a 64-slice MDCT scanner (LightSpeed Ultra, GE Healthcare, WI, USA) with the animals in the right lateral decubitus position. First, noncontrast CT images were obtained. Imaging parameters were: tube voltage=120kV, tube current=650mAs/slice, reconstructed slice thickness=4mm, spatial resolution=0.625×0.625×0.625mm. Additional images were obtained 3–5 minutes following the administration of iodinated CT contrast Omnipaque (350mg/ml, Omnipaque®, GE Healthcare, Princeton, NJ), which was injected as a bolus at a volume of 2ml/kg and at a rate of 5ml/s followed by a 40ml saline chase (using power injector).

Image Analysis

The qualitative appearance of the treated limbs was compared to each untreated contralateral limb on T1, T2, and postcontrast imaging. Specifically, the images were assessed for the presence of edema (as suggested by hyperintensity on T2-weighted images), bone marrow or cortical damage (as suggested by morphological irregularity, hypointensity, or hyperintensity on T1-weighted images at the bone-soft tissue interface), first-pass perfusion abnormalities (as suggested by abnormal enhancement/signal on the MR perfusion

sequences), and focal necrosis and/or abnormalities in local vascularity (as suggested by focal hypo- or hyperenhancement on postcontrast imaging). The maximum three plane dimensions of the hypoenhanced ablations (as seen on 10 minute postcontrast 3D LAVA images) were measured on a PACS workstation using available software (Impax, AGFA). The maximum intramedullary depth (MID) was measured on the coronal images by measuring the maximum transverse width of intramedullary hypoenhancement from the inner margin of the lateral cortex to the medial margin of hypoenhancement within the intramedullary space. Signal intensities were also measured in the region of each ablation on the first-pass perfusion images.

The CT images were assessed for cortical irregularity, abnormalities in marrow attenuation, abnormal enhancement, and abnormal soft tissue attenuation in the regions of the prescribed ablations. The ablations were not seen well enough by CT to calculate a specific ablation size on those images.

Statistical Analysis

The measurements were expressed as means ± standard deviation. The Mann-Whiteny test was used to compare the medians of the values. $P < 0.05$ was considered to indicate a statistically significant difference. Data analysis was performed with commercially available software (InStat 3.1a by GraphPad).

RESULTS

MRgHIFU was successfully used to produce sixteen focal bone ablations, two each, in the proximal and distal femoral diaphysis, respectively, in eight animals. Table 1 summarizes the sonication data per animal categorized by number of focal spots per ablation (six versus four) with associated minimum, maximum, and average energy per sonication, in addition to minimum, maximum, and average temperature rise per sonication.

Each focal bone ablation was characterized by an ovoid intramedullary and soft tissue rim of hyperintensity on T2-weighted images, suggesting edema, which corresponded to the target volume (Figure 2). T2-weighted MRI demonstrated muscle edema, while T1-weighted imaging demonstrated a thin rim of heterogenous mixed soft tissue signal abnormality adjacent to the distal ablations, suggesting cortical damage, but no abnormality adjacent to the proximal ablations. Post-contrast imaging demonstrated focal ovoid hypoenhancement of bone and soft tissue at the target volume with a thin rim of hyperenhancement. First-pass perfusion imaging failed to demonstrate the ablations later seen on the delayed postcontrast images. The similar regions of bone on the contralateral femurs appeared normal without any focal signal abnormalities or differential enhancement. Other than differences in the size of hypoenhancement, there were no significant qualitative differences in the appearance of the bone ablations and adjacent soft tissues following treatment among the sixteen ablations.

The average ablation sizes are summarized in Table 2. Maximum ablation length was measured on the postcontrast imaging in three dimensions (craniocaudal, transverse, and anteroposterior). Additionally, the maximum intramedullary depth (MID) was measured in the transverse dimension. The transverse ablation dimension was significantly larger in the

target volumes that received six compared to four sonications per slice (10.3 mm ± 1.2 compared to 7.0 mm ± 1.4 mm, p=0.002) (Figure 3). The increased length of the transverse dimension could be attributed essentially entirely to an increase in the MID in the animals that received 6 compared to 4 sonications (6.5 mm ± 0.9 compared to 2.9 mm ± 0.6, p<0.001). There was no significant difference in the size of the ablations between these two groups in the craniocaudal or anteroposterior dimension (p>0.05). Similar analysis of ablation size between high energy (distal) and low energy (proximal) ablations demonstrated no significant difference in the size of the ablation zone between the two groups (p>0.05). Finally, measurements of signal intensity in the region of the ablations during the acquisition of the first-pass perfusion images demonstrated no significant change in signal intensity from baseline over the course of imaging.

CT images performed with and without contrast media demonstrated no evidence of any structural abnormalities in either the bone or the adjacent skeletal muscle and no bony or soft tissue correlate to the ablations seen on MRI (Figure 4).

DISCUSSION

The major finding of this study is that the number of sonications used to ablate bone with MRgHIFU has a significant impact on the intramedullary depth of the ablation zone beyond the cortical surface. Differences in energy dose (and associated differences in temperature rise) did not have a significant affect on the hyperacute appearance of bone.

Additionally, our study suggested that MRI is superior to CT in visualizing ablations immediately after focused ultrasound treatment. In our study, the MRgHIFU ablations were best evaluated by T2-weighted fast spin echo sequences with fat saturation and postcontrast T1-weighted fast spoiled gradient echo imaging, in addition to MR thermometry sequences during the procedure. T1-weighted fast spin echo demonstrated subtle signal abnormalities in the region of the ablation. MRI first pass perfusion failed to demonstrate perfusion abnormalities at the ablations. The ablations were completely indiscernible on the acquired CT images, although advanced image reconstruction was not performed for CT.

The principal challenge in treating focal bone lesions is compensating for the marked attenuation of sound waves that happens at the interface with bone. While circumferential MRgHIFU targeting systems, such as those that have been developed for intracranial applications, have proven very effective, extensive variation in bone morphology makes it difficult to translate this approach broadly, particularly to the bones of the appendicular skeleton. We demonstrated that redundant and partially overlapping sonications within a prescribed treatment volume produced a significant increase in the maximum depth of the intramedullary ablation zone, without a qualitative difference in the appearance of the adjacent soft tissues. This result suggests the possibility of using repeat sonications in order to extend the depth of MRgHIFU treatment margins for focal bone lesions. This approach could allow for more complete ablation of subcortical lesions with wider treatment margins, in addition to increased access to central lesions within larger bones, which might otherwise be inaccessible to focused ultrasound sonications.

Focused ultrasound has gained popularity over the last decade in part because of its ability to generate thermal ablation foci with millimetric precision while sparing the integrity of adjacent structures (31). In most tissues, repeat focal sonications would be expected to create more well-defined foci of ablation at the target site, with minimal effect in the near or far-field of sonication where there is a rapid drop-off in energy. However, our study demonstrates that the unique far-field of MRgHIFU in bone is very sensitive to repeat sonications. Because bone absorbs a large fraction of sonication energy and requires a longer time for complete cooling (compared to soft tissue), the treated bone likely failed to return to baseline temperature between sonications. Repeated sonications likely resulted in a significantly increased energy dose to the far-field bone, with preferential extension of the ablation zone into the intramedullary space. In contrast, the near-field soft tissues attenuate relatively little of the sonication energy and there was no qualitative difference in the postablation appearance of the near-field soft tissues on multiple MRI sequences.

There was no significant difference in the postcontrast signal intensity or morphological appearance between high energy and low energy ablations. While our study was not sufficiently powered to detect very subtle differences in the post-HIFU appearance, this result suggests that lower energy might be sufficient for bone ablation, allowing for improved patient tolerance of MRgHIFU of bone.

This study was limited by the small sample size and the lack of histopathological correlation. However, the small sample size was partially mitigated by the use of the contralateral limb within the same field of view as a control for qualitative comparison. The study was also limited because we treated normal bone and our specific qualitative assessments and ablation size calculations might not apply to focal pathological lesions. Additionally, this study was limited to the femur as a representative of large bones and specific characterization of small bones or flat bones will require future studies. Finally, for purposes of specific statistical analyses, we grouped proximal and distal meta/diaphyseal ablations, making the assumption that these regions would respond similarly to focused sonications. However, subtle anatomical differences, particularly in vascularity, might have differentially impacted the post-ablation appearance.

In conclusion, sonication number during MR-guided HIFU of bone can be used to increase ablated volumes while energy dose had limited impact on size of created ablations. Overall MR-guided HIFU of bone can precisely control ablated volumes and minimize damage of adjacent soft tissue. MRI and MR thermometry are useful in evaluating the immediate effects of HIFU.

Acknowledgments

The authors would like to thank Ms. Nicole Bronson BSRT (R)(MR) and Ms. Carol Stillson, BA, VT for their technical support in imaging and animal preparation. The authors are also grateful for grant support from the National Institutes of Health (NIBIB T32 training grant 1 T32 EB001631)

Grant support: This research was supported by the National Institutes of Health (NIBIB T32 training grant 1 T32 EB001631) and a University of California San Francisco Department of Radiology and Biomedical Imaging Seed Grant.

References

1. Jolesz FA, Hynynen K, McDannold N, Tempany C. MR imaging-controlled focused ultrasound ablation: a noninvasive image-guided surgery. Magnetic resonance imaging clinics of North America. 2005; 13(3):545–560. [PubMed: 16084419]
2. Stewart EA, Gedroyc WM, Tempany CM, Quade BJ, Inbar Y, Ehrenstein T, Shushan A, Hindley JT, Goldin RD, David M, Sklair M, Rabinovici J. Focused ultrasound treatment of uterine fibroid tumors: safety and feasibility of a noninvasive thermoablative technique. Am J Obstet Gynecol. 2003; 189(1):48–54. [PubMed: 12861137]
3. Hindley J, Gedroyc WM, Regan L, Stewart E, Tempany C, Hynyen K, McDannold N, Inbar Y, Itzchak Y, Rabinovici J, Kim HS, Geschwind JF, Hesley G, Gostout B, Ehrenstein T, Hengst S, Sklair-Levy M, Shushan A, Jolesz F. MRI guidance of focused ultrasound therapy of uterine fibroids: early results. AJR Am J Roentgenol. 2004; 183(6):1713–1719. [PubMed: 15547216]
4. Catane R, Beck A, Inbar Y, Rabin T, Shabshin N, Hengst S, Pfeffer RM, Hanannel A, Dogadkin O, Liberman B, Kopelman D. MR-guided focused ultrasound surgery (MRgFUS) for the palliation of pain in patients with bone metastases–preliminary clinical experience. Ann Oncol. 2007; 18(1):163–167. [PubMed: 17030549]
5. Gianfelice D, Gupta C, Kucharczyk W, Bret P, Havill D, Clemons M. Palliative treatment of painful bone metastases with MR imaging–guided focused ultrasound. Radiology. 2008; 249(1):355–363. [PubMed: 18695209]
6. Liberman B, Gianfelice D, Inbar Y, Beck A, Rabin T, Shabshin N, Chander G, Hengst S, Pfeffer R, Chechick A, Hanannel A, Dogadkin O, Catane R. Pain palliation in patients with bone metastases using MR-guided focused ultrasound surgery: a multicenter study. Ann Surg Oncol. 2009; 16(1): 140–146. [PubMed: 19002530]
7. Dubinsky TJ, Cuevas C, Dighe MK, Kolokythas O, Hwang JH. High-intensity focused ultrasound: current potential and oncologic applications. AJR Am J Roentgenol. 2008; 190(1):191–199. [PubMed: 18094311]
8. Wu F, Wang ZB, Chen WZ, Zou JZ, Bai J, Zhu H, Li KQ, Jin CB, Xie FL, Su HB. Advanced hepatocellular carcinoma: treatment with high-intensity focused ultrasound ablation combined with transcatheter arterial embolization. Radiology. 2005; 235(2):659–667. [PubMed: 15858105]
9. Leslie T, Ritchie R, Illing R, Ter Haar G, Phillips R, Middleton M, Bch B, Wu F, Cranston D. High-intensity focused ultrasound treatment of liver tumours: post-treatment MRI correlates well with intra-operative estimates of treatment volume. Br J Radiol. 2012; 85(1018):1363–1370. [PubMed: 22700259]
10. Wu F, Wang ZB, Cao YD, Chen WZ, Bai J, Zou JZ, Zhu H. A randomised clinical trial of high-intensity focused ultrasound ablation for the treatment of patients with localised breast cancer. Br J Cancer. 2003; 89(12):2227–2233. [PubMed: 14676799]
11. Wu F, Wang ZB, Chen WZ, Bai J, Zhu H, Qiao TY. Preliminary experience using high intensity focused ultrasound for the treatment of patients with advanced stage renal malignancy. J Urol. 2003; 170(6 Pt 1):2237–2240. [PubMed: 14634387]
12. Illing RO, Kennedy JE, Wu F, ter Haar GR, Protheroe AS, Friend PJ, Gleeson FV, Cranston DW, Phillips RR, Middleton MR. The safety and feasibility of extracorporeal high-intensity focused ultrasound (HIFU) for the treatment of liver and kidney tumours in a Western population. Br J Cancer. 2005; 93(8):890–895. [PubMed: 16189519]
13. Murat FJ, Poissonnier L, Rabilloud M, Belot A, Bouvier R, Rouviere O, Chapelon JY, Gelet A. Mid-term results demonstrate salvage high-intensity focused ultrasound (HIFU) as an effective and acceptably morbid salvage treatment option for locally radiorecurrent prostate cancer. Eur Urol. 2009; 55(3):640–647. [PubMed: 18508188]
14. Ram Z, Cohen ZR, Harnof S, Tal S, Faibel M, Nass D, Maier SE, Hadani M, Mardor Y. Magnetic resonance imaging-guided, high-intensity focused ultrasound for brain tumor therapy. Neurosurgery. 2006; 59(5):949–955. discussion 955–946. [PubMed: 17143231]
15. Foley JL, Little JW, Starr FL 3rd, Frantz C, Vaezy S. Image-guided HIFU neurolysis of peripheral nerves to treat spasticity and pain. Ultrasound Med Biol. 2004; 30(9):1199–1207. [PubMed: 15550323]

16. Tsivgoulis G, Eggers J, Ribo M, Perren F, Saqqur M, Rubiera M, Sergentanis TN, Vadikolias K, Larrue V, Molina CA, Alexandrov AV. Safety and efficacy of ultrasound-enhanced thrombolysis: a comprehensive review and meta-analysis of randomized and nonrandomized studies. Stroke. 2010; 41(2):280–287. [PubMed: 20044531]
17. Lipsman N, Schwartz ML, Huang Y, Lee L, Sankar T, Chapman M, Hynynen K, Lozano AM. MR-guided focused ultrasound thalamotomy for essential tremor: a proof-of-concept study. Lancet Neurol. 2013; 12(5):462–468. [PubMed: 23523144]
18. Napoli A, Mastantuono M, Marincola BC, Anzidei M, Zaccagna F, Moreschini O, Passariello R, Catalano C. Osteoid Osteoma: MR-guided Focused Ultrasound for Entirely Noninvasive Treatment. Radiology. 2013
19. Li C, Wu P, Zhang L, Fan W, Huang J, Zhang F. Osteosarcoma: limb salvaging treatment by ultrasonographically guided high-intensity focused ultrasound. Cancer Biol Ther. 2009; 8(12): 1102–1108. [PubMed: 19448402]
20. Li C, Zhang W, Fan W, Huang J, Zhang F, Wu P. Noninvasive treatment of malignant bone tumors using high-intensity focused ultrasound. Cancer. 2010; 116(16):3934–3942. [PubMed: 20564113]
21. Chen W, Zhu H, Zhang L, Li K, Su H, Jin C, Zhou K, Bai J, Wu F, Wang Z. Primary bone malignancy: effective treatment with high-intensity focused ultrasound ablation. Radiology. 2010; 255(3):967–978. [PubMed: 20501734]
22. Bielack SS, Marina N, Bernstein M. High-intensity focused ultrasound (HIFU) is not indicated for treatment of primary bone sarcomas. Cancer. 2011
23. Konski A. High-intensity focused ultrasound in the treatment of bone tumors: another treatment option for palliation and primary treatment? Cancer. 2010; 116(16):3754–3755. [PubMed: 20564114]
24. Evans JA, Tavakoli MB. Ultrasonic attenuation and velocity in bone. Phys Med Biol. 1990; 35(10):1387–1396. [PubMed: 2243843]
25. Pinton G, Aubry JF, Bossy E, Muller M, Pernot M, Tanter M. Attenuation, scattering, and absorption of ultrasound in the skull bone. Med Phys. 2012; 39(1):299–307. [PubMed: 22225300]
26. Sikov MR. Effect of ultrasound on development. Part 1: Introduction and studies in inframammalian species. Report of the bioeffects committee of the American Institute of Ultrasound in Medicine. J Ultrasound Med. 1986; 5(10):577–583. [PubMed: 3534291]
27. Hynynen K, Clement G. Clinical applications of focused ultrasound-the brain. Int J Hyperthermia. 2007; 23(2):193–202. [PubMed: 17578343]
28. Tanter M, Pernot M, Aubry JF, Montaldo G, Marquet F, Fink M. Compensating for bone interfaces and respiratory motion in high-intensity focused ultrasound. Int J Hyperthermia. 2007; 23(2):141–151. [PubMed: 17578338]
29. Kopelman D, Inbar Y, Hanannel A, Pfeffer RM, Dogadkin O, Freundlich D, Liberman B, Catane R. Magnetic resonance guided focused ultrasound surgery. Ablation of soft tissue at bone-muscle interface in a porcine model. Eur J Clin Invest. 2008; 38(4):268–275. [PubMed: 18339007]
30. Rieke V, Butts Pauly K. MR thermometry. J Magn Reson Imaging. 2008; 27(2):376–390. [PubMed: 18219673]
31. Hynynen K. MRIgHIFU: a tool for image-guided therapeutics. J Magn Reson Imaging. 2011; 34(3):482–493. [PubMed: 22896850]

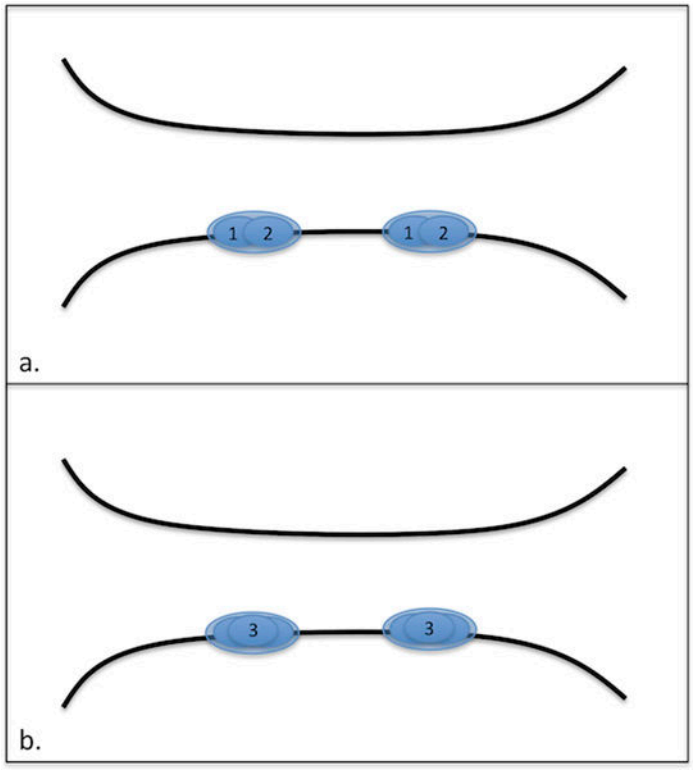

Figure 1.

(a) In four animals, two overlapping ovoid focal sonications were assigned to the proximal and distal ablations on two adjacent coronal slices. **(b)** In the remaining four animals, a third focal sonication was assigned between each pair of sonications (proximal and distal) on each of the two adjacent coronal slices.

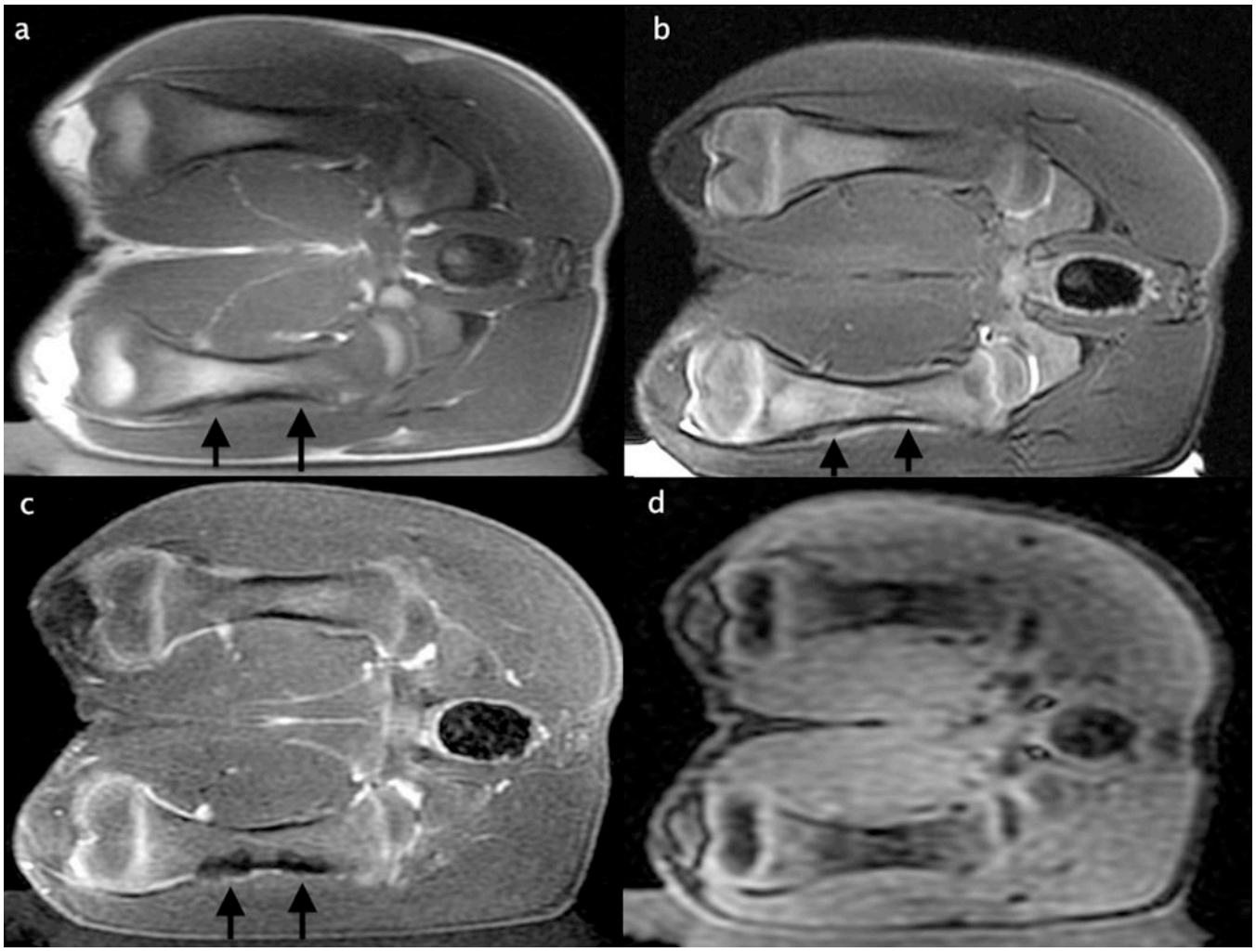

Figure 2.

Coronal **(a)** T2-weighted, **(b)** T1-weighted, **(c)** contrast enhanced T1 spoiled gradient echo and **(d)** perfusion MR images. The proximal and distal diaphysis of the right femur (downside limb) was sonicated. MR images were acquired immediately following HIFU ablation. The ablations are best seen on contrast enhanced T1 spoiled gradient echo imaging with two focal ovoid regions of hypoenhancement (arrows). Subtle T2 hyperintensity is noted along the diaphysis (arrows). Perfusion imaging failed to demonstrate the ablations.

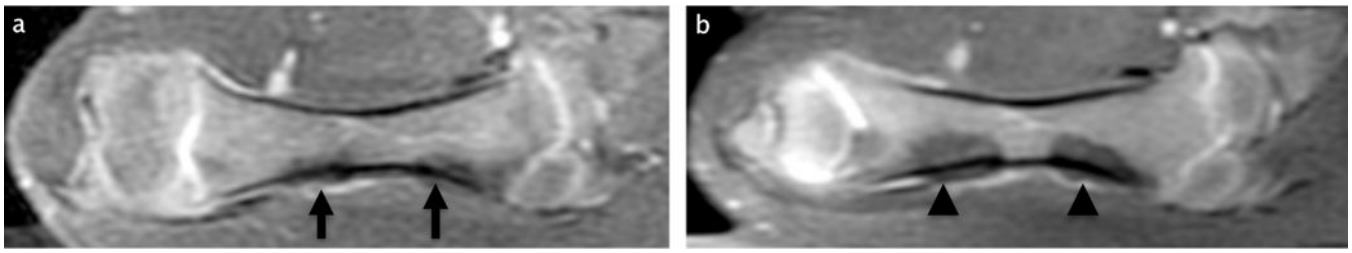

Figure 3.

Representative coronal contrast enhanced T1 spoiled gradient echo images obtained from two animals treated with either **(a)** two focal sonications per ablation (arrows) or **(b)** three focal sonications per ablations at this slice and the adjacent slice (arrowheads). There is substantial increase in the depth of the intramedullary hypoenhanced ablation zone after three focal sonications compared with two.

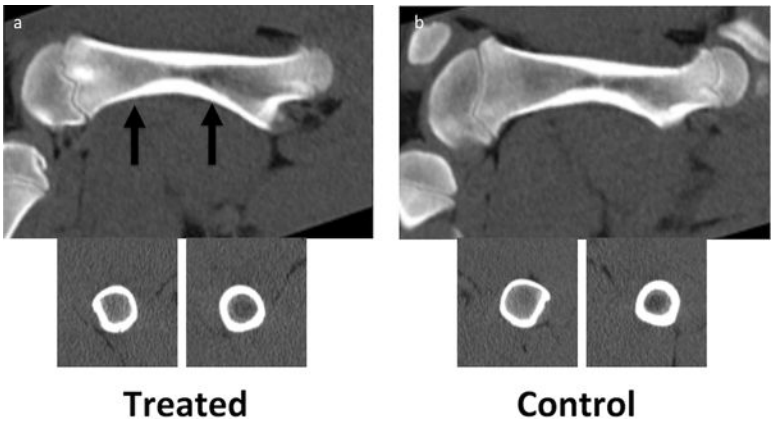

Figure 4.

Coronal (top row) reconstructions and axial (bottom row) contrast enhanced CT images acquired from treated femur (a) and contralateral control bone (b). Unlike MR imaging, this imaging modality failed to demonstrate the ablations at the sites of sonications immediately after treatment (arrows). Noncontrast CT showed no evidence of ablations.

Table 1

Sonication parameters for MRgHIFU for each animal.

		Proximal Ablation						Distal Ablation					
Animal ID	**Spots/ablation**	**Min J**	**Max J**	**Avg J**	**Min T**	**Max T**	**Avg T**	**Minimum J**	**Max J**	**Avg J**	**Min T**	**Max T**	**Avg T**
1	4	320	320	320	68	79	72.3	400	480	420	64	79	71.8
2	4	300	300	300	54	65	62.5	400	408	402	70	83	77.7
3	4	360	360	360	56	59	57.5	400	400	400	58	81	69.5
4	4	320	320	320	58	64	61.5	360	400	390	57	83	68.5
AVG ± SD	4	325 ± 25	325 ± 25	325 ± 25	59 ± 6	67 ± 9	64 ± 6	390 ± 20	422 ± 39	403 ± 13	62 ± 6	82 ± 2	72 ± 4
5	6	320	360	333	51	67	59.7	400	440	433	53	75	66.2
6	6	320	320	320	53	62	57.2	440	440	440	54	81	66.0
7	6	320	320	320	54	60	56.2	400	440	427	54	77	62.5
8	6	320	320	320	56	63	59.0	440	440	440	58	69	61.0
AVG ± SD	6	320 ± 0	330 ± 20	323 ± 7	54 ± 2	63 ± 3	58 ± 2	420 ± 23	440 ± 0	435 ± 6	55 ± 2	76 ± 5	64 ± 3

J, Joules; AVG, average; SD, standard deviation.

Table 2

MRgHIFU bone ablation sizes for each animal.

		Proximal Ablation				Distal Ablation			
Animal ID	**Spots/ablation**	**Transverse***	**CC**	**AP**	**MI***	**Transverse***	**CC**	**AP**	**MI***
1	4	6	20	17	2	8	19	16	3
2	4	6	21	16	3	6	20	14	3
3	4	8	22	17	3	6	22	16	3
4	4	9	19	16	4	6	21	17	2
AVG ± SD	4	7.3 ± 1.5	20.5 ± 1.3	12.5 ± 1.3	3.0 ± 0.8	6.5 ± 1.0	20.5 ± 1.3	12.3 ± 0.5	2.8 ± 0.5
5	6	11	22	18	7	12	23	18	8
6	6	11	21	16	6	11	21	16	7
7	6	9	22	16	7	9	22	14	6
8	6	10	21	15	6	9	21	17	5
AVG ± SD	6	10.3 ± 1.0	21.5 ± 0.6	13.0 ± 0.8	6.5 ± 0.6	10.3 ± 1.5	21.8 ± 1.0	13.3 ± 0.5	6.5 ± 1.3

CC, craniocaudal; AP, anteroposterior; MI, maximum intramedullary depth; AVG, average; SD, standard deviation.

*Denotes a significant difference in these dimensions between animals receiving 4 or 6 sonications per ablation ($P < 0.05$).